HHS Public Access

Author manuscript

Biochemistry. Author manuscript; available in PMC 2018 September 04.

Published in final edited form as:

Biochemistry. 2018 July 03; 57(26): 3599–3605. doi:10.1021/acs.biochem.8b00344.

Structural Plasticity in the C–Terminal Region of Macrophage Migration Inhibitory Factor–2 Is Associated with an Induced Fit Mechanism for a Selective Inhibitor

Georgios Pantouris[†], **Richard Bucala**[‡,§], and **Elias J. Lolis**[*,†,§]

[†]Department of Pharmacology, Yale School of Medicine, New Haven, Connecticut 06510, United States

[‡]Internal Medicine, Yale School of Medicine, New Haven, Connecticut 06510, United States

[§]Yale Cancer Center, Yale School of Medicine, New Haven, Connecticut 06510, United States

Abstract

We report the first reversible and selective small molecule inhibitor of pro-inflammatory protein macrophage migration inhibitory factor-2 (also known as MIF-2 or D-DT). 4-(3-Carboxyphenyl)-2,5pyridinedicarboxylic acid (4-CPPC) shows competitive binding with a 13fold selectivity for human MIF-2 versus human MIF-1. The crystal structure of MIF-2 complexed with 4-CPPC reveals an induced fit mechanism that is not observed in the numerous MIF-1/inhibitor complexes. Crystallographic analysis demonstrates the structural source of 4-CPPC binding and selectivity for MIF-2. 4-CPPC can be employed to reveal previously unrecognized functions of MIF-1 in biological systems in which both MIF-1 and MIF-2 are expressed, to improve our knowledge of the MIF family of proteins, and to provide new mechanistic insights that can be utilized for the development of potent and selective pharmacological modulators of MIF-2.

Graphical Abstract

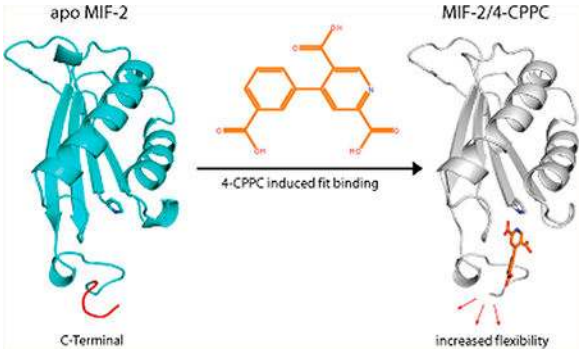

Human MIF-1 and MIF-2 are two immunoregulatory cytokines, are members of the same superfamily with similar structural properties, and have both overlapping and distinct

[*]Corresponding Author: elias.lolis@yale.edu.

Notes

The authors declare no competing financial interest.

biological functions. The crystal structure of human MIF-1 was the first to be determined in 1996 with the structure of MIF-2 determined three years later.[1,2] The biological assembly of both proteins is homotrimeric with a solvent channel along the 3-fold axis and a conserved catalytic base, P1, at the N-terminus. Via this catalytic residue, MIF-1 and MIF-2 catalyze the tautomerization of natural (p-hydroxyphenylpyruvate and phenylpyruvate) and synthetic molecules (Ddopachrome and its derivatives).[3,4] Whether *p*-hydroxyphenyl-pyruvate (HPP) or phenylpyruvate is the physiological substrate for MIFs is still under debate, though HPP and D-dopachrome have been used as model substrates in many studies. Intriguingly, despite sharing the same substrates, MIF-1 and MIF-2 differ in both their active site environments and catalytic efficiencies.[5] Numerous small molecule inhibitors of the MIF-1 tautomerase activity have been identified as competitive,[6] noncompetitive,[7] and covalent inhibitors.[8,9] In contrast, the suicide inhibitor, 4-iodo-6-phenylpyrimidine (4IPP), which covalently modifies P1 of both MIF-1 and MIF-2, is the only known inhibitor of MIF-2.[5]

MIF-1 and MIF-2 are localized in the cytoplasm and exported to the extracellular space after cell activation to bind and signal through the CD74/CD44 cell surface receptor complex.[4,10] Binding of MIF-1 or MIF-2 to the CD74/CD44 complex triggers the ERK1/2 MAP kinase signaling cascade that leads to various downstream responses, including chemotaxis, proliferation, and inhibition of apoptosis.[4] Experimental three-dimensional structures of MIF-1 and MIF-2 with their receptor, CD74, have yet to be determined, though molecular models are available for both complexes.[11,12] Chemical modifications, site-directed mutagenesis, and recent structural modeling studies indicate that CD74 activation is dependent on residues at the interface between two subunits, outside the catalytic cavity of the MIF proteins.[9,11–13] Recent mechanistic insights into the MIF-1-induced activation of CD74 showed that the activation process is dynamically controlled by an allosteric site that is found on one side of the solvent channel.[14] Whether a similar allosteric site exists for MIF-2 has yet to be explored. MIF-1 also activates chemokine receptors CXCR2 and CXCR4 leading to cell cycle arrest, integrin activation, chemotaxis, and calcium influx.[15] The MIF-1 activation sites for CXCR2 and CXCR4 are already defined.[16,17] Activation of chemokine receptors by MIF-2 has not yet been shown.

Whereas MIF-1 is a validated clinical target with an anti-MIF antibody in clinical studies,[23–25] the precise contribution of MIF-2 to physiology and pathology is less characterized than that of MIF-1. The functional role of MIF-1 and MIF-2 in various tissues and cell types is not well understood and is the subject of active research. For instance, in cardiac surgery that involves myocardial ischemia/reperfusion, MIF-1 and MIF-2 have opposite functions.[18] While increased levels of MIF-1 during cardiac surgery play an organ-protective role, high levels of MIF-2 are associated with the development of heart dysfunction. In cancer, MIF-1 and MIF-2 were shown to share tumorigenic and pro-inflammatory properties. Immunoneutralization of MIF-1 and MIF-2 protects from invasive cancer and lethal systemic inflammation.[4,19] Gene knockdown studies suggest that the two proteins have cooperative deleterious actions in transformed cells,[4,20,21] and in a study of renal cell carcinoma, MIF-2 exhibited a pro-tumorigenic effect that was more dramatic than that of MIF-1.[22]

In this study, we describe 4-CPPC as the first reversible and selective inhibitor of MIF-2. Binding of 4-CPPC takes place via a major conformational change of the C-terminal region of MIF-2. This compound can provide the foundation for identifying chemical analogues that serve as potent inhibitors of MIF-2 activity for studying the protein's role in pathology as well as for examining the synergistic effects of MIF-1 and MIF-2 in immune physiology.

METHODS

Expression and Purification of MIF-1 and MIF-2.

Expression and purification of MIF-1 have been described elsewhere.[9,26] Briefly, BL21 Gold (DE3) *Escherichia coli* cells were transformed with a pET-11b plasmid that expresses MIF-1, grown at 37 °C to an OD_{600} of 0.6, and induced with isopropyl β-D-1-thiogalactopyranoside (IPTG). For MIF-1 purification, the cells were resuspended in 20 mM Tris (pH 7.4) and 20 mM NaCl, lysed using sonication, and purified using Q-and SP-Sepharose columns connected in series. MIF-1 (~95% pure) was eluted in the flow through. The small amount of contamination was removed using 16/60 Superdex 75. For MIF-2, the pET-22b plasmid containing the cDNA of the protein was transformed in BL21 Gold (DE3) E. coli cells. The cells were grown at 37 °C to an OD_{600} of 0.6, induced using IPTG at a final concentration of 1 mM, and lysed using sonication in 20 mM Tris (pH 8.5) and 20 mM NaCl (buffer A). The supernatant was loaded onto a Q-Sepharose column (120 mL) and extensively washed with ~1.1 L of buffer A, and MIF-2 was eluted with 5% buffer B [20 mM Tris (pH 8.5) and 1 M NaCl]. The protein was concentrated and loaded onto an 16/60 Superdex 75 column (120 mL) using 20 mM Tris (pH 7.4) and 150 mM NaCl as the running buffer. This step offers partial purification of the protein and also results in buffer exchange. Finally, the Q-Sepharose step was repeated once more using a gradient elution (0–20% buffer B).

Crystallization of the MIF-2/4-CPPC Complex and Structure Determination.

The discovery of 4-CPPC by *in silico* screening and its functional characterization are described elsewhere (R. Bucala, manuscript in preparation). The crystal structure of MIF-2 in complex with 4-CPPC was obtained by soaking apo-MIF-2 crystals in 4-CPPC. Crystals of apo-MIF-2 were obtained using the hanging drop method in 24-well trays. Two microliters of apo-MIF-2, at 10 mg/mL, was mixed with an equal volume of the well solution containing 28%–34% (w/ v) PEG 4000, 0.1 M sodium citrate (pH 5.8), and 0.2 M ammonium acetate. Crystals at their maximum size were obtained from trays stored at 20 °C within a week. For soaking experiments, apo-MIF-2 crystals were transferred to preequilibrated drops containing 35% (w/v) PEG 4000, 0.1 M sodium citrate (pH 5.8), 0.2 M ammonium acetate, and 0.2 M 4-CPPC. After being incubated for 24 h, the soaked crystals were flash-frozen without a cryoprotectant and tested for diffraction at the Yale School of Medicine Macromolecular Xray Facility using a Rigaku Pilatus 200K Detector with a Rigaku 007 rotating copper anode X-ray generator (wavelength of 1.5418 Å). The data set was collected to 1.40 Å at a temperature of 100 K, integrated, and scaled using the HKL2000 program suite.[27] The initial model of the MIF-2/4CPPC complex was obtained by molecular replacement using the CCP4-supported program Molrep.[28] The crystal structure of apo-MIF-2 [Protein Data Bank (PDB) entry 1DPT] was used as the search model,

resulting in a clear $F_o - F_c$ map for 4-CPPC that was generated by the CCP4-supported program FFT[32] and visualized in PyMOL.[2,33] The coordinates (PDB) and crystallographic information file (CIF) of 4-CPPC were produced by PRODRG.[31] Refinement of the structure was performed using Refmac[29] and COOT.[30] Ramachandran analysis of the MIF-2/4-CPPC complex demonstrated 0% outliers and 97.6% amino acids in the preferred regions. The biological assembly of the MIF-2/4-CPPC complex was generated by PISA[34] and PyMOL. Interactions between MIF2 and 4-CPPC were analyzed by PyMOL. Superimposition of the MIF-2/4-CPPC crystal structure on the corresponding structure of apo-MIF-2 was performed by the CCP4-supported program SUPERPOSE,[28] resulting in a root-mean-square deviation (RMSD) of 0.28 Å. The apo-MIF-1 crystal structure (PDB entry 3DJH) was aligned with the MIF-2/4-CPPC structure by PyMOL, resulting in a RMSD of 1.29 Å. The MIF2/4-CPPC structure has been deposited in the PDB as entry 6C5F.

Tautomerase Assays.

For measurement of the potency of 4-CPPC against MIF-1 or MIF-2 keto/enol HPP enzymatic activity, a 100 mM stock solution of *p*-hydroxyphenylpyruvate (HPP) was freshly prepared in 50 mM ammonium acetate (pH 6.2) and incubated overnight at room temperature to favor formation of the HPP keto form. A mixture containing borate at a final concentration of 0.420 M, MIF-1 or MIF-2 at a final concentration of 100 or 250 nM, respectively, and 4-CPPC in dimethyl sulfoxide (DMSO) was transferred to an ultraviolet transparent flat bottom 96-well plate containing HPP at final concentrations between 0 and 2 mM. The final DMSO concentration was 1%. The formation of the HPP enol-borate complex was measured at 306 nm (ε_{306} = 11400 M^{-1} cm^{-1}) for a total of 90 s. All the experiments were performed in triplicate.

RESULTS

Kinetic and Structural Characterization of 4-CPPC Binding to MIF-2.

To characterize 4-CPPC, we performed the HPP inhibition assay on both MIF-1 and MIF-2. We found that 4-CPPC inhibits MIF-1 and MIF-2 with K_i values of 431 ± 37 and 33 ± 0.7 μM, respectively, with a 13-fold selectivity for MIF-2 (Figure 1). Other than 4-IPP that inhibits both MIF-1 and MIF-2 via covalent inhibition, 4-CPPC is the first selective inhibitor for MIF-2 with a competitive mode of binding (Figure 1).

To provide more information about the binding mode of the compound and its selectivity for MIF-2, the crystal structure of MIF-2 in complex with 4-CPPC was determined at 1.4 Å (Figure 2). Our experimental analysis revealed that the pyridine-2,5-dicarboxylic acid moiety of 4-CPPC is buried in the active site pocket of MIF-2 and has a critical role in stabilizing the MIF-2/4-CPPC complex, as a result of the electrostatic, hydrogen-bond, and hydrophobic interactions that are formed with active site residues (Figure 3 a-c). The two carboxylate groups of pyridine-2,5-dicarboxylic acid moiety form electrostatic interactions with K32, R36, and K109 as well as strong hydrogen-bond interactions with P1, S63, I64, and K109 (Figure 3b,c). 4-CPPC is also stabilized via polar interactions with S63 and S104 and hydrophobic interactions with P1, F2, I64, and I107 (Figure 3b). While most of the

compound is found inside the catalytic pocket, the benzoic acid moiety of 4-CPPC is not, with the third carboxylate group and part of the benzene ring exposed to solvent (Figure 3a).

Induced Fit Mode of Inhibition by 4-CPPC.

To probe changes upon binding of 4-CPPC, we superimposed the apoMIF-2 and MIF-2/4-CPPC crystal structures. Despite the high level of superposition agreement between the two structures (RMSD of 0.28 Å) (Figure 4a), close examination of the active site region demonstrated distinct differences that provide insights into 4-CPPC binding. Through an induced fit mechanism, C-terminal residues V113–L117 of MIF-2 become flexible moving from their original apo-MIF-2 position to create an open conformation for accommodating 4-CPPC in the active site pocket. In the presence of 4-CPPC, V113 was found to be significantly shifted from its apo-form position while electron densities for residues M114–L117 were not detected, indicating the increased mobility of this region (Figure 4a). Further analysis shows that the position of M114 in the apo structure, which faces the catalytic residue P1, would clash with the position of 4-CPPC (Figure 4a). Consequently, residues become dynamic when 4-CPPC interacts with the active site pocket. The currently described induced fit mechanism with disordered residues for MIF-2 inhibition by 4-CPPC is not observed in the crystal structure of the MIF-2/4IPP or MIF-2/ tartrate complex (Figure 4b) or in the large number of MIF-1 structures complexed with competitive (e.g., ISO-1),[6] noncompetitive (e.g., AV411),[7] and covalent inhibitors (e.g., MIF1)[9] as well as an N-terminal insertion, three alanine residues inserted between P1 and M2 (PA_3M). The polyalanine insertion has increased the mobility relative to that of wildtype MIF-1 and is located close to the C-terminal region.[9] Even in the case of p425, an allosteric inhibitor that binds on the surface of MIF-1 and interacts directly with the C-terminal region,[35] there are no conformational changes.

4-CPPC Selectivity for MIF-2.

We are also interested in understanding the structural basis of 4-CPPC selectivity for MIF-2 versus MIF-1. To explain the kinetic data, we aligned the MIF-2/4-CPPC crystal structure with that of MIF-1 (PDB entry 3DJH) and compared the two active site residues within a 5 Å radius around the inhibitor. One of the first conclusions had to do with the dissimilar amino acid composition of the two active sites. Only three active site residues (P1, K32, and I64) were found to be common for both proteins. The MIF-1 active site is less polar and has more aromatic residues (Y36, Y95, W108, and F113) in the corresponding positions where MIF-2 has R36, L96, K109, and V113 (Figure 5a). These differences in amino acid composition influence the shape and polarity of the two active sites. Molecules with negatively charged moieties, like 4-CPPC, favor binding to the MIF-2 active site because of its electropositive potential. Crystallographic analysis demonstrates that binding of 4-CPPC in the active site of MIF-1 is partly obstructed by three residues. F113 clashes with the benzoic acid moiety of 4-CPPC, while Y36 and Y95 are closer to 4-CPPC than van der Waals interactions allow (Figure 5b). These three residues are bulky, affecting the orientation and binding of 4-CPPC in the active site pocket of MIF-1. From these findings, it is apparent that pharmacophores with negative charges can be used for the development of more selective MIF-2 inhibitors.

DISCUSSION

Upregulation of the human MIF protein family, MIF-1 and MIF-2, plays a role in various disorders.[18,36–39] Characterization of the compound 4-IPP against both MIF-1 and MIF-2 indicated there are substantial differences in how this compound interacts with each protein.[5] For example, the kinetics of covalent formation is 2-fold faster with complete inactivation of MIF-1 as opposed to MIF-2 where total inactivation does not occur. In addition, structural studies indicated that the 6-phenylpyrimidine (6-PP) adduct occupies the active site of MIF-1, whereas 6-PP, in MIF-2, is tethered by the covalent bond to P1 to occupy a site outside the catalytic cavity. Despite these differences, 4-IPP lacks specificity and therefore cannot serve as a tool for studying the distinct effects of MIF-1 or MIF-2. It is therefore important to develop reagents that can be used to decipher the contribution of each protein in physiology or disease.

Herein, we report the first selective inhibitor for MIF-2, which is characterized by an in vitro kinetic assay and X-ray crystallography analysis. Binding of 4-CPPC occurs via an induced fit mechanism, in which C-terminal residues V113– L117 of MIF-2 undergo major conformational changes to accommodate binding of 4-CPPC in the catalytic pocket. Inspection of a large number of human MIF-1/inhibitor cocrystal structures shows that the C-terminal region of MIF-1 does not undergo a conformational change resulting in dynamic motion. The strong hydrogen bonds made between 4-CPPC and MIF-2 contrast with the lower potency of the compound. The induced fit model of MIF-2 inhibition might explain the low potency of 4-CPPC with an increase in energy to “displace” four C-terminal residues. 4-CPPC demonstrates selectivity for MIF-2 and can be used for understanding the function of MIF2. In addition, our study provides insight for increasing the affinity and selectivity of 4-CPPC for MIF-2 to design a better reagent. Examination of the residues that surround 4-CPPC in the active site of MIF-2 indicates a number of modifications that could optimize the potency of this compound. As discussed above, the pyridine-2,5-dicarboxylic acid moiety forms hydrogen bonds and electrostatic interactions with active site residues, while the benzoic acid moiety of 4-CPPC faces toward the solvent, does not interact with the protein, and probably has a minimal impact. Therefore, structure–activity relationships and structure-based design on the benzoic acid group of 4-CPPC can increase the potency and selectivity of the inhibitor.

Acknowledgments

Funding

This work was supported by the Robert E. Leet and Clara Guthrie Patterson Trust Fellowship Program in Clinical Research, Bank of America, N.A., Trustee (G.P.), and National Institutes of Health Grants AI065029, AI082295 (E.J.L.), and S10-OD018007-01 (instrumentation grant).

ABBREVIATIONS

MIF	macrophage migration inhibitory factor
D-DT	D-dopachrome tautomerase
4-CPPC	4-(3-carboxyphenyl)-2,5pyridinedicarboxylic acid

HPP	4-(hydroxyphenyl) pyruvate
4IPP	4-iodo-6-phenylpyrimidine
6-PP	6-phenylpyrimidine
PDB	Protein Data Bank
RMSD	root-mean-square deviation
DMSO	dimethyl sulfoxide

REFERENCES

(1). Sun HW, Bernhagen J, Bucala R, and Lolis E (1996) Crystal structure at 2.6-A resolution of human macrophage migration inhibitory factor. *Proc. Natl. Acad. Sci. U. S. A.* 93, 5191–5196. [PubMed: 8643551]

(2). Sugimoto H, Taniguchi M, Nakagawa A, Tanaka I, Suzuki M, and Nishihira J (1999) Crystal structure of human D-dopachrome tautomerase, a homologue of macrophage migration inhibitory factor, at 1.54 A resolution. Biochemistry 38, 3268–3279. [PubMed: 10079069]

(3). Swope M, Sun HW, Blake PR, and Lolis E (1998) Direct link between cytokine activity and a catalytic site for macrophage migration inhibitory factor. EMBO J. 17,3534–3541. [PubMed: 9649424]

(4). Merk M, Zierow S, Leng L, Das R, Du X, Schulte W, Fan J, Lue H, Chen Y, Xiong H, Chagnon F, Bernhagen J, Lolis E, Mor G, Lesur O, and Bucala R (2011) The D-dopachrome tautomerase (DDT) gene product is a cytokine and functional homolog of macrophage migration inhibitory factor (MIF). Proc. Natl. Acad. Sci. U. S. A 108, E577–585. [PubMed: 21817065]

(5). Rajasekaran D, Zierow S, Syed M, Bucala R, Bhandari V, and Lolis EJ (2014) Targeting distinct tautomerase sites of D-DT and MIF with a single molecule for inhibition of neutrophil lung recruitment. FASEB J. 28, 4961–4971. [PubMed: 25016026]

(6). Lubetsky JB, Dios A, Han J, Aljabari B, Ruzsicska B, Mitchell R, Lolis E, and Al-Abed Y (2002) The tautomerase active site of macrophage migration inhibitory factor is a potential target for discovery of novel anti-inflammatory agents. J. Biol. Chem 277, 24976–24982. [PubMed: 11997397]

(7). Cho Y, Crichlow GV, Vermeire JJ, Leng L, Du X, Hodsdon ME, Bucala R, Cappello M, Gross M, Gaeta F, Johnson K, and Lolis EJ (2010) Allosteric inhibition of macrophage migration inhibitory factor revealed by ibudilast. Proc. Natl. Acad. Sci. U. S. A 107, 11313–11318. [PubMed: 20534506]

(8). Crichlow GV, Fan C, Keeler C, Hodsdon M, and Lolis EJ (2012) Structural interactions dictate the kinetics of macrophage migration inhibitory factor inhibition by different cancer-preventive isothiocyanates. Biochemistry 51, 7506–7514. [PubMed: 22931430]

(9). Pantouris G, Syed MA, Fan C, Rajasekaran D, Cho TY, Rosenberg EM, Jr., Bucala R, Bhandari V, and Lolis EJ (2015) An Analysis of MIF Structural Features that Control Functional Activation of CD74. Chem. Biol 22, 1197–1205. [PubMed: 26364929]

(10). Merk M, Mitchell RA, Endres S, and Bucala R (2012) Ddopachrome tautomerase (D-DT or MIF-2): Doubling the MIF cytokine family. *Cytokine*+ 59, 10–17. [PubMed: 22507380]

(11). Meza-Romero R, Benedek G, Leng L, Bucala R, and Vandenbark AA (2016) Predicted structure of MIF/CD74 and RTL1000/CD74 complexes. Metab. Brain Dis 31, 249–255. [PubMed: 26851955]

(12). Meza-Romero R, Benedek G, Jordan K, Leng L, Pantouris G, Lolis E, Bucala R, and Vandenbark AA (2016) Modeling of both shared and distinct interactions between MIF and its homologue D-DT with their common receptor CD74. *Cytokine*+ 88, 62–70. [PubMed: 27573366]

(13). Singh AK, Pantouris G, Borosch S, Rojanasthien S, and Cho TY (2017) Structural basis for decreased induction of class IB PI3-kinases expression by MIF inhibitors. J. Cell Mol. Med 21, 142–153. [PubMed: 27619729]

(14). Pantouris G, Ho J, Shah D, Syed MA, Leng L, Bhandari V, Bucala R, Batista VS, Loria JP, and Lolis E (2018) Nanosecond Dynamics Regulate the MIF-Induced Activity of CD74. *Angew. Chem., Int. Ed.*, n/a.

(15). Bernhagen J, Krohn R, Lue H, Gregory JL, Zernecke A, Koenen RR, Dewor M, Georgiev I, Schober A, Leng L, Kooistra T, Fingerle-Rowson G, Ghezzi P, Kleemann R, McColl SR, Bucala R, Hickey MJ, and Weber C (2007) MIF is a noncognate ligand of CXC chemokine receptors in inflammatory and atherogenic cell recruitment. Nat. Med 13, 587–596. [PubMed: 17435771]

(16). Lacy M, Kontos C, Brandhofer M, Hille K, Groning S, Sinitski D, Bourilhon P, Rosenberg E, Krammer C, Thavayogarajah T, Pantouris G, Bakou M, Weber C, Lolis E, Bernhagen J, and Kapurniotu A (2018) Identification of an Arg-LeuArg tripeptide that contributes to the binding interface between the cytokine MIF and the chemokine receptor CXCR4. Sci. Rep 8, 5171. [PubMed: 29581527]

(17). Weber C, Kraemer S, Drechsler M, Lue H, Koenen RR, Kapurniotu A, Zernecke A, and Bernhagen J (2008) Structural determinants of MIF functions in CXCR2-mediated inflammatory and atherogenic leukocyte recruitment. Proc. *Natl. Acad. Sci. U. S. A.* 105, 16278–16283. [PubMed: 18852457]

(18). Stoppe C, Rex S, Goetzenich A, Kraemer S, Emontzpohl C, Soppert J, Averdunk L, Sun Y, Rossaint R, Lue H, Huang C, Song Y, Pantouris G, Lolis E, Leng L, Schulte W, Bucala R, Weber C, and Bernhagen J (2015) Interaction of MIF Family Proteins in Myocardial Ischemia/ Reperfusion Damage and Their Influence on Clinical Outcome of Cardiac Surgery Patients. Antioxid. Redox Signaling 23, 865–879.

(19). Kobold S, Merk M, Hofer L, Peters P, Bucala R, and Endres S (2014) The macrophage migration inhibitory factor (MIF)homologue D-dopachrome tautomerase is a therapeutic target in a murine melanoma model. Oncotarget 5, 103–107. [PubMed: 24406307]

(20). Coleman AM, Rendon BE, Zhao M, Qian M-W, Bucala R, Xin D, and Mitchell RA (2008) Cooperative regulation of nonsmall cell lung carcinoma angiogenic potential by macrophage migration inhibitory factor and Its homolog, D-dopachrome tautomerase. J. Immunol 181, 2330–2337. [PubMed: 18684922]

(21). Brock SE, Rendon BE, Yaddanapudi K, and Mitchell RA (2012) Negative regulation of AMP-activated protein kinase (AMPK) Activity by macrophage migration inhibitory factor (MIF) family members in non-small cell lung carcinomas. J. Biol. Chem 287, 37917–37925. [PubMed: 22988252]

(22). Pasupuleti V, Du W, Gupta Y, Yeh IJ, Montano M, Magi-Galuzzi C, and Welford SM (2014) Dysregulated D-dopachrome Tautomerase, a Hypoxia-inducible Factor-dependent Gene, Cooperates with Macrophage Migration Inhibitory Factor in Renal Tumorigenesis. J. Biol. Chem 289, 3713–3723. [PubMed: 24356968]

(23). Bucala R (2013) MIF, MIF alleles, and prospects for therapeutic intervention in autoimmunity. J. Clin. Immunol 33 (Suppl. 1), 72–78.

(24). Kerschbaumer RJ, Rieger M, lkel D, Le Roy D, Roger T, Garbaraviciene J, Boehncke W-H, Müllberg J, Hoet RM, Wood CR, Antoine G, Thiele M, Savidis-Dacho H, Dockal M, Ehrlich H, Calandra T, and Scheiflinger F (2012) Neutralization of Macrophage Migration Inhibitory Factor (MIF) by Fully Human Antibodies Correlates with Their Specificity for the β-Sheet Structure of MIF. J. Biol. Chem 287, 7446–7455. [PubMed: 22238348]

(25). Phase 2a Study of BAX69 and 5-FU/Leucovorin or Panitumumab Versus Standard of Care in Subjects With Metastatic Colorectal Cancer, October 23, 2017. National Institutes of Health (ClinicalTrials.gov).

(26). Pantouris G, Rajasekaran D, Garcia AB, Ruiz VG, Leng L, Jorgensen WL, Bucala R, and Lolis EJ (2014) Crystallographic and receptor binding characterization of Plasmodium falciparum macrophage migration inhibitory factor complexed to two potent inhibitors. J. Med. Chem 57, 8652–8656. [PubMed: 25268646]

(27). Otwinowski Z, and Minor W (1997) [20] Processing of X-ray diffraction data collected in oscillation mode. Methods Enzymol. 276, 307–326.

(28). Winn MD, Ballard CC, Cowtan KD, Dodson EJ, Emsley P, Evans PR, Keegan RM, Krissinel EB, Leslie AG, McCoy A, McNicholas SJ, Murshudov GN, Pannu NS, Potterton EA, Powell HR,

Read RJ, Vagin A, and Wilson KS (2011) Overview of the CCP4 suite and current developments. Acta Crystallogr., Sect. D: Biol. Crystallogr 67, 235–242. [PubMed: 21460441]

(29). Winn MD, Murshudov GN, and Papiz MZ (2003) Macromolecular TLS refinement in REFMAC at moderate resolutions. Methods Enzymol. 374, 300–321. [PubMed: 14696379]

(30). Emsley P, and Cowtan K (2004) Coot: model-building tools for molecular graphics. Acta Crystallogr., Sect. D: Biol. Crystallogr 60, 2126–2132. [PubMed: 15572765]

(31). Schuttelkopf AW, and van Aalten DMF (2004) PRODRG: a tool for high-throughput crystallography of protein-ligand complexes. Acta Crystallogr., Sect. D: Biol. Crystallogr 60, 1355–1363. [PubMed: 15272157]

(32). Murshudov GN, Vagin AA, Lebedev A, Wilson KS, and Dodson EJ (1999) Efficient anisotropic refinement of macromolecular structures using FFT. Acta Crystallogr., Sect. D: Biol. Crystallogr 55, 247–255. [PubMed: 10089417]

(33). DeLano WL (2002) The PyMOL molecular graphics system, DeLano Scientific, Palo Alto, CA.

(34). Krissinel E, and Henrick K (2007) Inference of Macromolecular Assemblies from Crystalline State. J. Mol. Biol 372, 774–797. [PubMed: 17681537]

(35). Bai F, Asojo OA, Cirillo P, Ciustea M, Ledizet M, Aristoff PA, Leng L, Koski RA, Powell TJ, Bucala R, and Anthony KG (2012) A novel allosteric inhibitor of macrophage migration inhibitory factor (MIF). J. Biol. Chem 287, 30653–30663. [PubMed: 22782901]

(36). Pohl J, Hendgen-Cotta UB, Stock P, Luedike P, and Rassaf T (2017) Elevated MIF-2 levels predict mortality in critically ill patients. J. Crit. Care 40, 52–57. [PubMed: 28329734]

(37). Guo D, Guo J, Yao J, Jiang K, Hu J, Wang B, Liu H, Lin L, Sun W, and Jiang X (2016) D-dopachrome tautomerase is overexpressed in pancreatic ductal adenocarcinoma and acts cooperatively with macrophage migration inhibitory factor to promote cancer growth. Int. J. Cancer 139, 2056–2067. [PubMed: 27434219]

(38). Wang Q, Wei Y, and Zhang J (2017) Combined Knockdown of D-dopachrome Tautomerase and Migration Inhibitory Factor Inhibits the Proliferation, Migration, and Invasion in Human Cervical Cancer. International journal of gynecological cancer: official journal of the International Gynecological Cancer Society 27, 634–642. [PubMed: 28338494]

(39). Benedek G, Meza-Romero R, Jordan K, Zhang Y, Nguyen H, Kent G, Li J, Siu E, Frazer J, Piecychna M, Du X, Sreih A, Leng L, Wiedrick J, Caillier SJ, Offner H, Oksenberg JR, Yadav V, Bourdette D, Bucala R, and Vandenbark AA (2017) MIF and D-DT are potential disease severity modifiers in male MS subjects. Proc. Natl. Acad. Sci. U. S. A 114, E8421–e8429. [PubMed: 28923927]

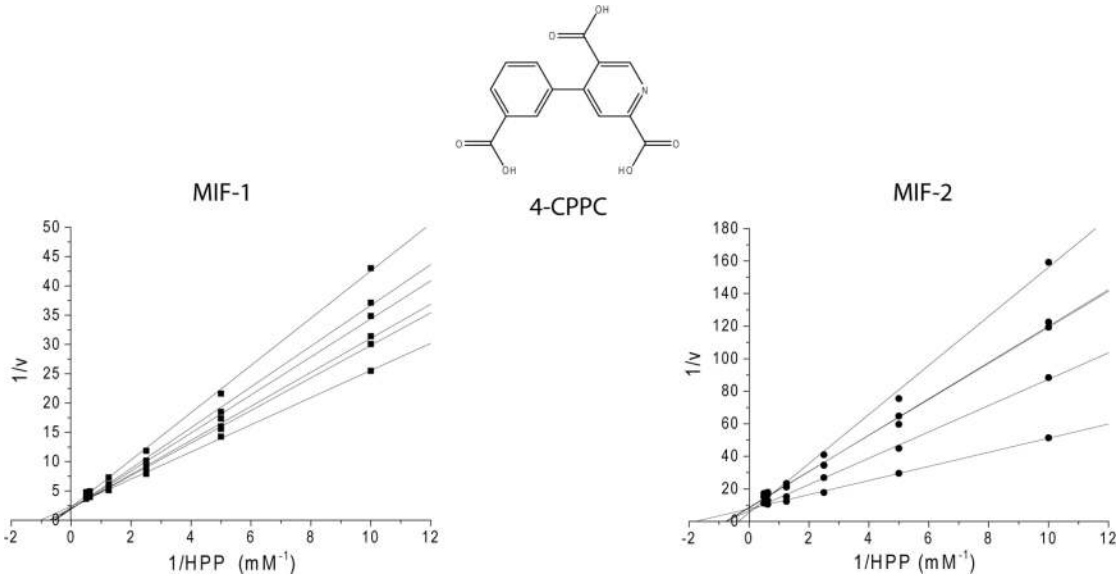

Figure 1.
Lineweaver–Burk plots of MIF-1 and MIF-2 with 4-CPPC.

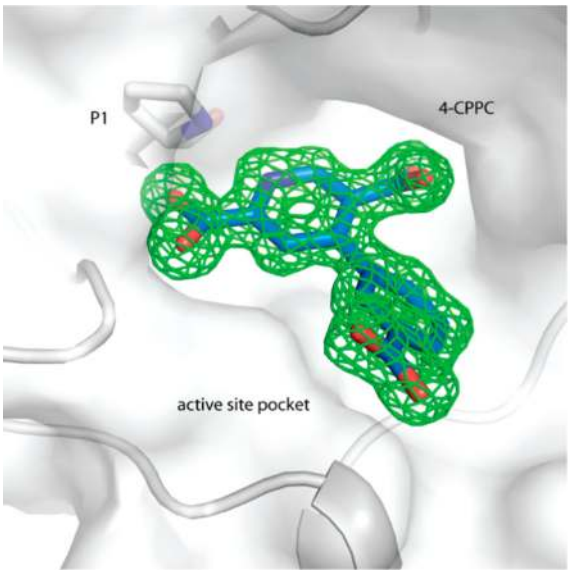

Data collection	
Space group	P 3
Cell dimensions	
a, *b*, *c* (Å)	83.94, 83.94, 40.48
α, β, γ (°)	90.00, 90.00, 120.00
Resolution (Å)	50.00-1.40 (1.42-1.40) *
R_{sym} or R_{merge}	0.04 (0.147)
I / σI	80.3 (13.8)
Completeness (%)	100.0 (100.0)
Redundancy	7.9 (5.2)
Refinement	
Resolution (Å)	41.97-1.40
No. reflections	60002
R_{work} / R_{free}	0.12/0.16
No. atoms	
Protein	2589
Ligand/ion	21
Water	404
B-factors	
Protein	14
Ligand/ion	17
Water	31
R.m.s. deviations	
Bond lengths (Å)	0.025
Bond angles (°)	2.010

*Values in parentheses are for highest-resolution shell

Figure 2.

Crystallographic analysis of the MIF-2/4-CPPC complex obtained at 1.4 Å. On the left side, the unbiased $F_o - F_c$ electron density map of 4-CPPC (green) is observed at 3σ. P1 and 4-CPPC are shown as gray and blue sticks, respectively. The X-ray crystallographic statistics of the MIF-2/4-CPPC complex are given in the table.

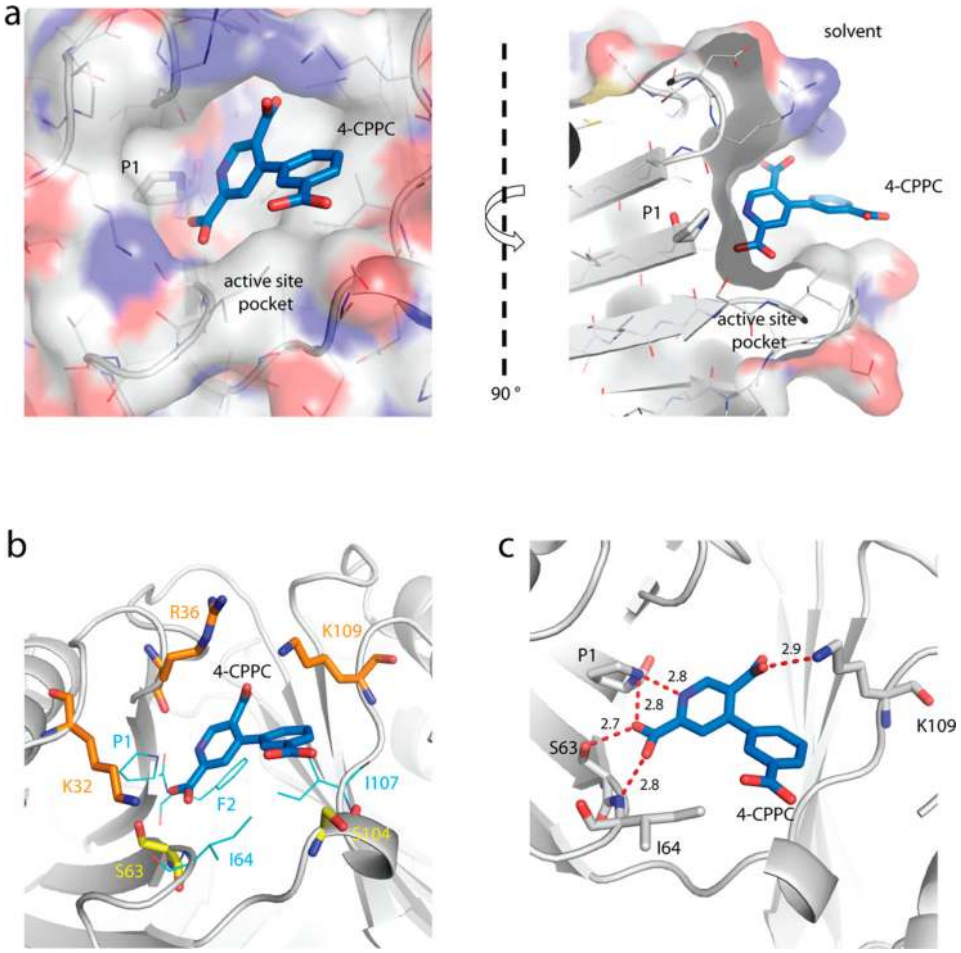

Figure 3.

Crystallographic analyses of 4-CPPC binding in the active site of MIF-2. (a) Crystallographic studies reveal the binding motif of 4-CPPC in the active site of MIF-2. P1 and 4-CPPC are shown as gray and blue sticks, respectively. The active site pocket is illustrated as a gray cavity in the 90 °C rotation at the right. (b) 4-CPPC forms electrostatic interactions with K32, R36, and K109 (orange sticks for carbon atoms), polar interactions with S63 and S104 (yellow sticks), and hydrophobic interactions with P1, F2, I64, and I107 (cyan lines). (c) 4-CPPC forms strong hydrogen-bond interactions with P1, S63, I64, and K109 (gray sticks).

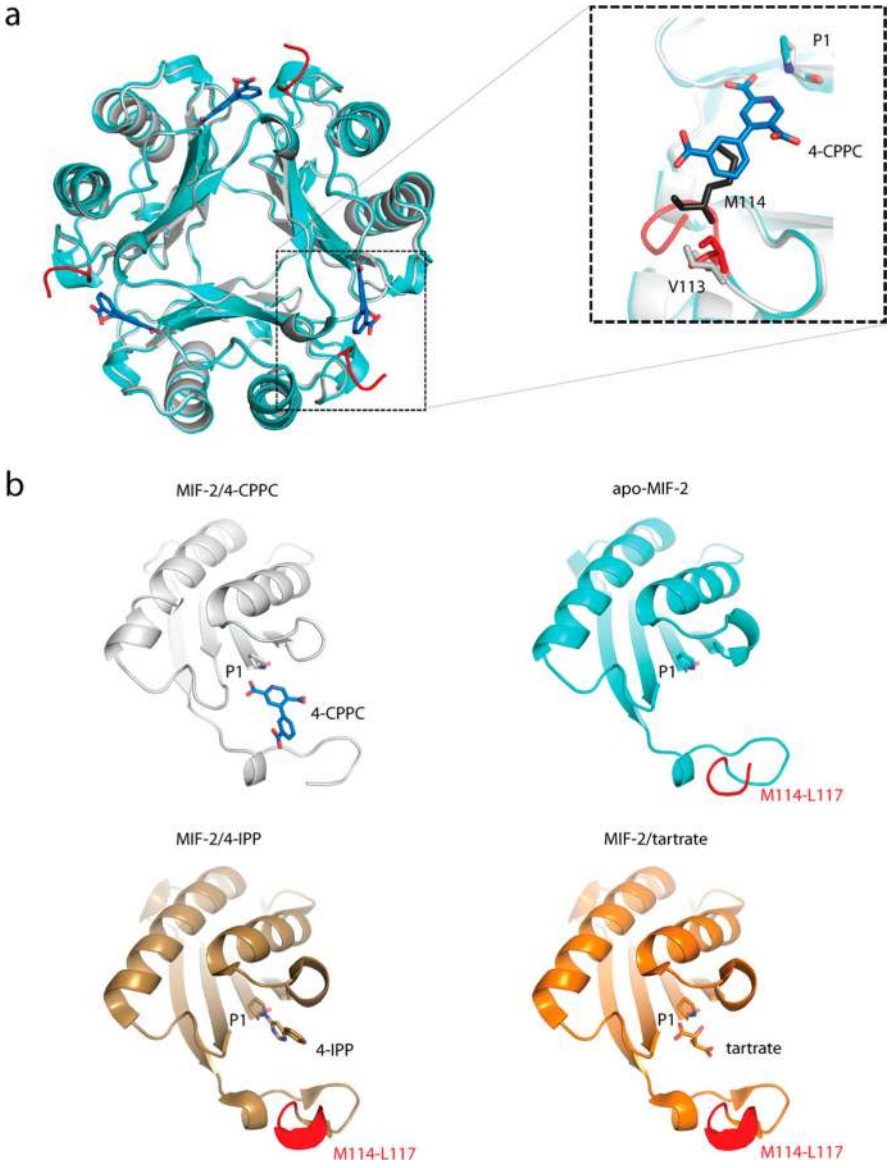

Figure 4.

Induced fit mechanism of MIF-2 inhibition by 4-CPPC. (a) The induced fit mechanism of 4-CPPC binding involves major conformational changes of C-terminal residues V113–L117, with no electron density for residues M114–L117, indicating that this region becomes flexible when 4CPPC binds to the active site of MIF-2. The superposed crystal structures of the apo-MIF-2 and MIF-2/4-CPPC complexes are colored cyan and gray, respectively, while 4-CPPC is shown as blue sticks. In the apo-MIF-2 crystal structure, the V113–L117 loop is colored red. In the MIF-2/4CPPC structure, V113 is the last residue with complete electron density but its side chain orientation is different from that of apo-MIF-2; V113 is shown as gray and red sticks for MIF-2/4-CPPC and apo-MIF-2, respectively. M114 of the apo-MIF-2 crystal structure is shown as black sticks. In the presence of 4-CPPC, M114 in the apo-MIF-2 conformation would clash. P1 is also shown as sticks. (b) Comparison of the MIF-2/4-CPPC crystal structure (gray) with the corresponding structures of apo-MIF-2

(cyan), MIF-2/4-IPP (brown), and MIF-2/tartrate (orange). Residues M114–L117 are colored red, while ligands and P1 are shown as sticks.

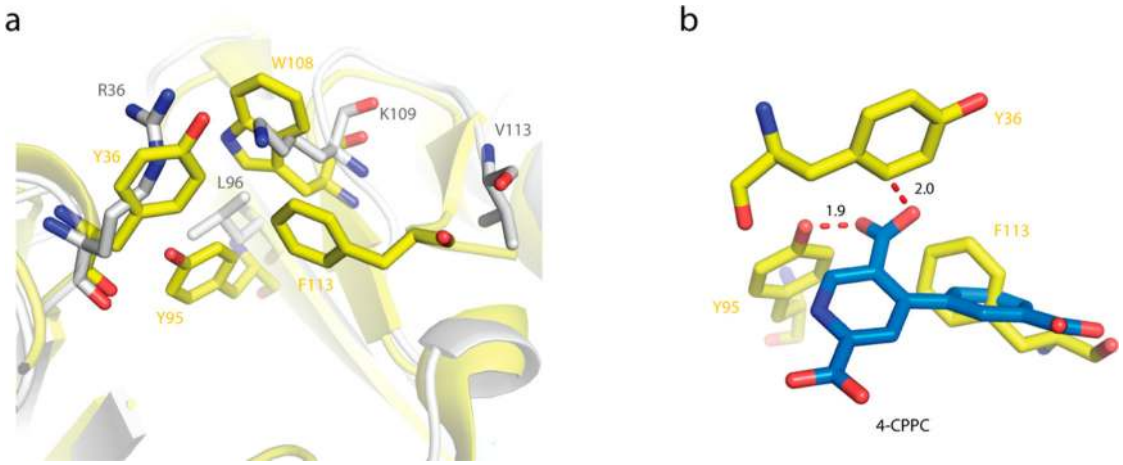

Figure 5.

Structural basis of 4-CPPC selectivity for MIF-2 vs MIF-1. (a) Comparison between the aligned apo-MIF-1 (yellow) and MIF-2/4-CPPC (gray) crystal structures reveals major differences in the shape and polarity of the two active sites. Y36, Y95, W108, and F113 of MIF-1 and the corresponding residues of MIF-2 (R36, L96, K109, and V113, respectively) are shown as sticks. (b) Selectivity of 4-CPPC for MIF-2 over MIF-1 is derived from residue F113 of MIF-1, which clashes with the compound, while Y36 and Y95 are located in the proximity. Y36, Y95, and F113 of the crystal structure of apo-MIF-1 are presented as yellow sticks. 4-CPPC of the crystal structure of the MIF-2/4-CPPC complex is displayed as blue sticks.